
Finding the Needle in the Haystack with Convolutions: on the benefits of architectural bias

Stéphane d’Ascoli

stephane.dascoli@ens.fr

Laboratoire de Physique de l’Ecole normale supérieure ENS, Université PSL,
CNRS, Sorbonne Université, Université Paris-Diderot, Sorbonne Paris Cité, Paris, France

Levent Sagun

leventsagun@fb.com

Facebook AI Research
Facebook, Paris, France

Joan Bruna

bruna@cims.nyu.edu

Courant Institute of Mathematical Sciences and Center for Data Science
New York University, New York City, United States

Giulio Biroli

giulio.biroli@lps.ens.fr

Laboratoire de Physique de l’Ecole normale supérieure ENS, Université PSL,
CNRS, Sorbonne Université, Université Paris-Diderot, Sorbonne Paris Cité, Paris, France

Abstract

Despite the phenomenal success of deep neural networks in a broad range of learning tasks, there is a lack of theory to understand the way they work. In particular, Convolutional Neural Networks (CNNs) are known to perform much better than Fully-Connected Networks (FCNs) on spatially structured data: the architectural structure of CNNs benefits from prior knowledge on the features of the data, for instance their translation invariance. The aim of this work is to understand this fact through the lens of dynamics in the loss landscape.

We introduce a method that maps a CNN to its equivalent FCN (denoted as eFCN). Such an embedding enables the comparison of CNN and FCN training dynamics directly in the FCN space. We use this method to test a new training protocol, which consists in training a CNN, embedding it to FCN space at a certain “relax time”, then resuming the training in FCN space. We observe that for all relax times, the deviation from the CNN subspace is small, and the final performance reached by the eFCN is higher than that reachable by a standard FCN of same architecture. More surprisingly, for some intermediate relax times, the eFCN outperforms the CNN it stemmed, by combining the prior information of the CNN and the expressivity of the FCN in a complementary way. The practical interest of our protocol is limited by the very large size of the highly sparse eFCN. However, it offers interesting insights into the persistence of architectural bias under stochastic gradient dynamics. It shows the existence of some rare basins in the FCN loss landscape associated with very good generalization. These can only be accessed thanks to the CNN prior, which helps navigate the landscape during the early stages of optimization.

1 Introduction

In the classic dichotomy between model-based and data-based approaches to solving complex tasks, Convolutional Neural Networks (CNN) correspond to a particularly efficient tradeoff. CNNs capture key geometric prior information for spatial/temporal tasks through the notion of local translation invariance. Yet, they combine this prior with high flexibility, that allows them to be scaled to millions of parameters and leverage large datasets with gradient-descent learning strategies, typically operating in the ‘interpolating’ regime, i.e. where the training data is fit perfectly.

Such regime challenges the classic notion of model selection in statistics, whereby increasing the number of parameters trades off bias by variance [39]. On the one hand, several recent works studying the role of optimization in this tradeoff argue that model size is not always a good predictor for overfitting [31, 39, 30, 18, 7], and consider instead other complexity measures of the function class, which favor CNNs due to their smaller complexity [14]. On the other hand, authors have also considered geometric aspects of the energy landscape, such as width of basins [25], as a proxy for generalisation. However, these properties of the landscape do not appear to account for the benefits associated with specific architectures. Additionally, considering the implicit bias due to the optimization scheme [36, 21] is not enough to justify the performance gains without considering the architectural bias. Despite the important insights on the role of over-parametrization in optimization [13, 3, 37], the architectural bias prevails as a major factor to explain good generalization in visual classification tasks – over-parametrized CNN models generalize well, but large neural networks without any convolutional constraints do not.

In this work, we attempt to further disentangle the bias stemming from the architecture and the optimization scheme by showing that the CNN prior plays a favorable role mostly at the *beginning* of optimization. Geometrically, the CNN prior defines a low-dimensional subspace within the space of parameters of generic Fully-Connected Networks (FCN) (this subspace is linear since the CNN constraints of weight sharing and locality are linear, see Figure 1 for a sketch of the core idea). Even though the optimization scheme is able to minimize the training loss with or without the constraints (for sufficiently over-parametrized models [19, 39]), the CNN subspace provides a “better route” that navigates the loss landscape to solutions with better generalization performance.

Yet, surprisingly, we observe that leaving this subspace at an appropriate time can result in a FCN with an equivalent or even better generalization than a CNN. Our numerical experiments suggest that the CNN subspace *as well as* its vicinity are good candidates for high-performance solutions. Furthermore, we observe a threshold distance from the CNN space beyond which the performance drops back down to the vanilla FCN accuracy level. Our results offer a new perspective on the success of the convolutional architecture: within FCN loss landscapes there exist rare basins associated to very good generalization, characterised not only by their width but rather by their distance to the CNN subspace. These can be accessed thanks to the CNN prior, and are otherwise missed in the usual training of FCNs.

The rest of the paper is structured as follows. Section 2 discusses prior work in relating architecture and optimization biases. Section 3 presents our CNN to FCN embedding algorithm and training procedure, and Section 4 describes and analyses the experiments performed on the CIFAR-10 dataset [26]. We conclude in Section 5 by describing theoretical setups compatible with our observations and consequences for practical applications.

2 Related Work

The relationship between CNNs and FCNs is an instance of trading-off prior information with expressivity within Neural Networks. There is abundant literature that explored the relationship between different neural architectures, for different purposes. One can roughly classify these works on whether they attempt to map a large model into a smaller one, or vice-versa.

In the first category, one of the earliest efforts to introduce structure within FCNs with the goal of improving generalization was Nowlan and Hinton’s soft weight sharing networks [33], in which the weights are regularized via a Mixture of Gaussians. Another highly popular line of work attempts to *distill* the “knowledge” of a large model (or an ensemble of models) into a smaller one [8, 23, 4], with the goal of improving both computational efficiency and generalization performance. Network

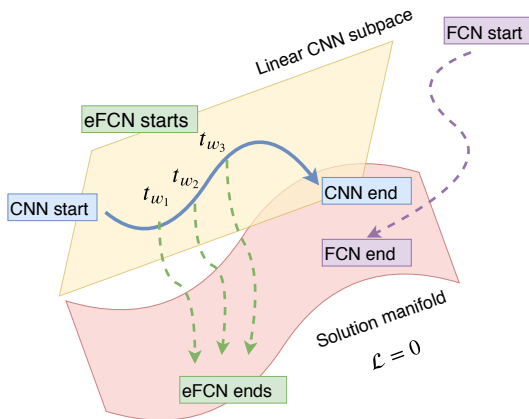


Figure 1: **White background:** ambient, M -dimensional, fully-connected space. **Yellow subspace:** linear, m -dimensional convolutional subspace. We have $m \ll M$. **Red manifold:** (near-) zero loss valued, (approximate-) solution set for a given training data. Note that it is a nontrivial manifold due to continuous symmetries (also, see the related work section on mode connectivity) and it intersects with the CNN subspace. **Blue path:** a CNN initialized and trained with the convolutional constraints. **Purple path:** a FCN model initialized and trained without the constraints. **Green paths:** Snapshots taken along the CNN training that are lifted to the ambient FCN space, and trained in the FCN space without the constraints.

pruning [22] and the recent “Lottery Ticket Hypothesis” [15] are other remarkable instances of the benefits of model reduction.

In the second category, which is more directly related to our work, authors have attempted to build larger models by embedding small architectures into larger ones, such as the Net2Net model [10] or more evolved follow-ups [35]. In these works, however, the motivation is to accelerate learning by some form of knowledge transfer between the small model and the large one, whereas our motivation is to understand the specific role of architectural bias in generalization.

In the infinite-width context, [32] study the role of translation equivariance of CNNs compared to FCNs. They find that in this limit, weight sharing does not play any role in the Bayesian treatment of CNNs, despite providing significant improvement in the finite-channel setup.

The links between generalization error and the geometry and topology of the optimization landscape have been also extensively studied in recent times. [14] compare generalisation bounds between CNNs and FCNs, establishing a sample complexity advantage in the case of linear activations. [29, 28] obtain specific generalisation bounds for CNN architectures. [9] proposed a different optimization objective, whereby a bilateral filtering of the landscape favors dynamics into wider valleys. [25] explored the link between sharpness of local minima and generalization through Hessian analysis [34], and [38] argued in terms of the volume of basins of attraction. The characterization of the loss landscape along paths connecting different models have been studied recently, e.g. in [16], [17], and [12]. The existence of rare basins leading to better generalization was found and highlighted in simple models in [5, 6]. The role of the CNN prior within the ambient FCNs loss landscape and its implication for generalization properties were not considered in any of these works. In the following we address this point by building on these previous investigations of the landscape properties.

3 CNN to FCN Embedding

In both FCNs and CNNs, each feature of a layer is calculated by applying a non-linearity to a weighted sum over the features of the previous layer (or over all the pixels of the image, for the first layer). CNNs are a particular type of FCNs, which make use of two key ingredients to reduce their number of redundant parameters: locality and weight sharing.

Locality: In FCNs, the sum is taken over all the features of the previous layer. In locally connected networks (LCNs), locality is imposed by restricting the sum to a small receptive field (a box of adjacent features of the previous layer). The set of weights of this restricted sum is called a filter. For a given receptive field, one may create multiple features (or channels) by using several different filters. This procedure makes use of the spatial structure of the data and reduces the number of fitting parameters.

Weight sharing: CNNs are a particular type of LCNs where all the filters of a given channel use the same set of weights. This procedure makes use of the somewhat universal properties of feature

extracting filters such as edge detectors and reduces even more drastically the number of fitting parameters.

When mapping a CNN to its equivalent FCN (eFCN), we obtain very sparse (due to locality) and redundant (due to weight sharing) weight matrices (see Sec. A of the Supplemental Material for some intuition on the mapping). This typically results in a large memory overhead as the eFCN of a simple CNN can take several orders of magnitude more space in the memory. Therefore, we present the core ideas on a simple 3-layer CNN on CIFAR-10 [27], and show similar results for AlexNet on CIFAR-100 in Sec. B of the Supplemental Material.

In the mapping¹, all layers apart from the convolutional layers (ReLU, Dropout, MaxPool and fully-connected) are left unchanged except for proper reshaping. Each convolutional layer is mapped to a fully-connected layer.

As a result, for a given CNN, we obtain its eFCN counterpart with an end-to-end fully-connected architecture which is functionally identical to the original CNN.

4 Experiments

We are given input-label pairs for a supervised classification task, (x, y) , with $x \in \mathbb{R}^d$ and y the index of the correct class for a given image x . The network, parametrized by θ , outputs $\hat{y} = f_x(\theta)$. To distinguish between different architectures we denote the CNN weights by $\theta^{CNN} \in \mathbb{R}^M$ and the eFCNs weights by $\theta^{eFCN} \in \mathbb{R}^M$. Let's denote the embedding function described in Sec. 3 by $\Phi : \mathbb{R}^m \mapsto \mathbb{R}^M$ where $m \ll M$ and with a slight abuse of notation use $f(\cdot)$ for both CNN and eFCN. Dropping the explicit input dependency for simplicity we have:

$$f(\theta^{CNN}) = f(\Phi(\theta^{CNN})) = f(\theta^{eFCN}).$$

For the experiments, we prepare the CIFAR-10 dataset for training without data augmentation. The optimizer is set to stochastic gradient descent with a constant learning rate of 0.1 and a minibatch size of 250. We turn off the momentum and weight decay to simply focus on the stochastic gradient dynamics and we do not adjust the learning rate throughout the training process. In the following, we focus on a convolutional architecture with 3 layers, 64 channels at each layer that are followed by ReLU and MaxPooling operators, and a single fully connected layer that outputs prediction probabilities. In our experience, this VanillaCNN strikes a good balance of simplicity and performance in that its equivalent FCN version does not suffer from memory issues yet it significantly outperforms any FCN model trained from scratch. We study the following protocol:

1. Initialize the VanillaCNN at θ_{init}^{CNN} and train for 150 epochs. At the end of training θ_{final}^{CNN} reaches $\sim 72\%$ test accuracy.
2. Along the way, save k snapshots of the weights at logarithmically spaced epochs: $\{t_0 = 0, t_1, \dots, t_{k-2}, t_{k-1} = 150\}$. It provides k CNN points denoted by $\{\theta_{t_0}^{CNN} = \theta_{init}^{CNN}, \theta_{t_1}^{CNN}, \dots, \theta_{t_{k-1}}^{CNN}\}$.
3. Lift each one to its eFCN: $\{\Phi(\theta_{t_0}^{CNN}), \dots, \Phi(\theta_{t_{k-1}}^{CNN})\} = \{\theta_{t_0}^{eFCN}, \dots, \theta_{t_{k-1}}^{eFCN}\}$ (so that only m among a total of M parameters are non-zero).
4. Train these k eFCNs in the FCN space for 100 epochs in the same conditions, except a smaller learning rate of 0.01. We obtain k solutions $\{\theta_{t_0, final}^{eFCN}, \dots, \theta_{t_{k-1}, final}^{eFCN}\}$.
5. For comparison, train a standard FCN (with the same architecture as the eFCNs but with the default PyTorch initialization) for 100 epochs in the same conditions as the eFCNs, and denote the resulting weights by θ_{final}^{FCN} . The latter reaches $\sim 55\%$ test accuracy.

This process gives us one CNN solution, one FCN solution, and k eFCN solutions that are labeled as

$$\theta_{final}^{CNN}, \theta_{final}^{FCN}, \text{ and } \{\theta_{t_0, final}^{eFCN}, \dots, \theta_{t_{k-1}, final}^{eFCN}\} \quad (1)$$

which we analyze in the following subsections. Note that due to the difference in size between the CNN and the eFCNs, it unclear what learning rate would give a fair comparison. One solution, shown in Sec. B of the Supplemental Material, is to use an adaptive learning rate optimizer such as Adam.

¹The source code may be found at: <https://github.com/sdascoli/anarchitectural-search>.

4.1 Performance and training dynamics of eFCNs

Our first aim is to characterize the training dynamics of eFCNs and study how their training evolution depends on their *relax time* $t_w \in \{t_0 = 0, t_1, \dots, t_{k-2}, t_{k-1} = 150\}$ (in epochs). When the architectural constraint is relaxed, the loss decreases monotonically to zero (see the left panel of Fig. 2). The initial losses are smaller for larger t_w s, as expected since those t_w s correspond to CNNs trained for longer. In the right panel of Fig. 2, we show a more surprising result: test accuracy increases monotonously in time for all t_w s, thus showing that *relaxing the constraints does not lead to overfitting or catastrophic forgetting*. Hence, from the point of view of the FCN space, it is not as if CNN dynamics took place on an unstable region from which the constraints of locality and weight sharing prevented from falling off. It is quite the contrary instead: the CNN dynamics takes place in a basin, and when the constraints are relaxed, the system keeps going down on the training surface and up in test accuracy, as opposed to falling back to the standard FCN regime.

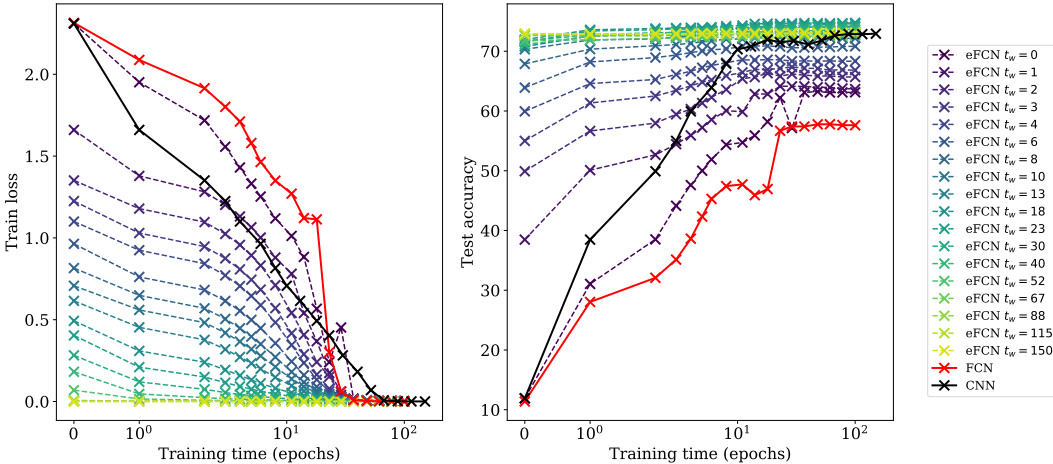


Figure 2: Training loss (**left**) and test accuracy (**right**) on CIFAR-100 vs. training time in logarithmic scale including the initial point. Different models are color coded as follows: the VanillaCNN is shown in black, standard FCN is in red, and the eFCNs with their relax time t_w s are indicated by the gradient ranging from purple to light green.

In Fig. 3 (left) we compare the final test accuracies reached by eFCN with the ones of the CNN and the standard FCN. We find two main results. First, the accuracy of the eFCN for $t_w = 0$ is approximately at 62.5%, well above the standard FCN result of 57.5%. This shows that imposing an *untrained* CNN prior is already enough to find a solution with much better performance than a standard FCN. Hence the CNN prior brings us to a good region of the landscape *to start with*. The second result, perhaps even more remarkable, is that at intermediate relax times ($t_w \sim 20$ epochs), the eFCN reaches—and exceeds—the final test accuracy reached by the CNN it stemmed from. This supports the idea that the constraints are mostly helpful for navigating the landscape *during the early stages of optimization*. At late relax times, the eFCN is initialized close to the bottom of the landscape and has little room to move, hence the test accuracy stays the same as that of the fully trained CNN.

Interestingly, very similar observations were made in a concurrent paper [20] which studies the effect of early relaxing of regularization procedures such as weight decay and data augmentation. They relate this phenomenology to an early "critical period" of learning during which regularization is most important.

4.2 A closer look at the landscape

A widespread idea in the deep learning literature is that the sharpness of the minima of the training loss is related to generalization performance [25, 24]. The intuition being that flat minima reduce the effect of the difference between training loss and test loss. This motivates us to compare the first and second order properties of the landscape explored by the eFCNs and the CNNs they stem from. To do so, we investigate the norm of the gradient of the training loss, $|\nabla \mathcal{L}|$, and the top eigenvalue of the

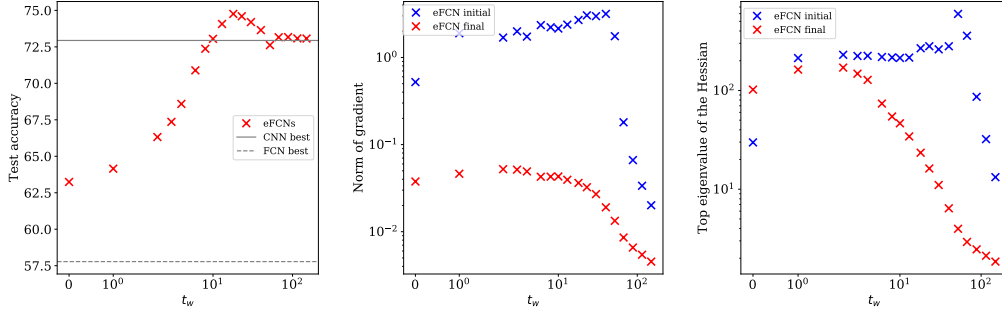


Figure 3: **Left:** Performance of eFCNs reached at the end of training (red crosses) compared to its counterpart for the best CNN accuracy (straight line) and the best FCN accuracy (dashed line). **Center:** Norm of the gradient for eFCNs at the beginning and at the end of training. **Right:** Largest eigenvalue of the Hessian for eFCNs at the beginning and at the end of training. In all figures the x -axis is the relax time t_w .

Hessian of the training loss, λ_{max} , in the central and right panels of Fig. 3 (we calculate the latter using a power method).

We point out several interesting observations. First, the sharpness ($|\nabla\mathcal{L}|$) and steepness (λ_{max}) indicators increase then decrease during the training of the CNN (as analyzed in [1]), and display a maximum around $t_w \simeq 20$, which coincides with the relax time of best improvement for the eFCNs. Second, we see that after training the eFCNs, these indicators plummet by an order of magnitude, which is particularly surprising at very late relax time where it appeared in the left panel of Fig. 3 (see also 4) as if the eFCNs was hardly moving away from initialization. This supports the idea that when the constraints are relaxed, the extra degrees of freedom *lead us to wider basins*, possibly explaining the gain in performance.

4.3 How far does the eFCN escape from the CNN subspace?

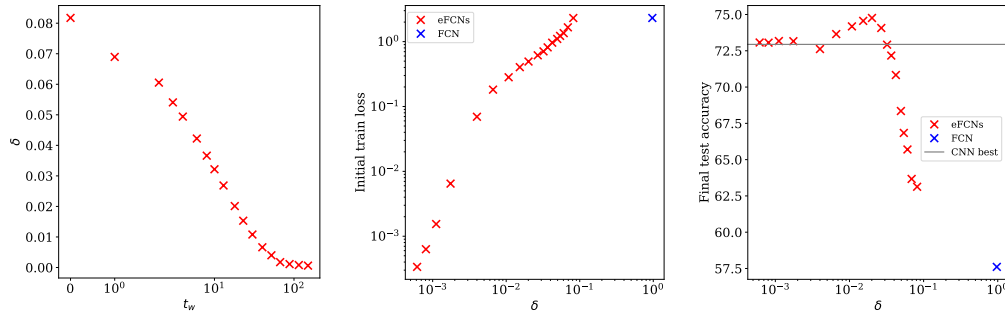


Figure 4: **Left panel:** relax time t_w of the eFCN vs. δ , the measure of deviation from the CNN subspace through the locality constraint, at the final point of eFCN training. **Middle panel:** δ vs. the initial loss value. **Right panel:** δ vs. final test accuracy of eFCN models. For reference, the blue point in the **middle** and **right** panels indicate the deviation measure for a standard FCN, where $\delta \sim 97\%$.

A major question naturally arises: how far do the eFCNs move away from their initial condition? Do they stay close to the sparse configuration they were initialized in? To answer this question, we quantify how locality is violated once the constraints are relaxed (violation of weight sharing will be studied in Sec. 4.4). To this end, we consider a natural decomposition of the weights in the FCN space into two parts, $\theta = (\theta_{local}, \theta_{off-local})$, where $\theta_{off-local} = 0$ for an eFCN when it is initialized from a CNN. A visualization of these blocks may be found in Sec. A of the Supplemental Material. We

then study the ratio δ of the norm of the off-local weights to the total norm, $\delta(\theta) = \frac{\|\theta_{\text{off-local}}\|_2}{\|\theta\|_2}$, which is a measure of the deviation of the model from the CNN subspace.

Fig. 4 (left) shows that the deviation δ at the end of eFCN training decreases monotonically with its relax time t_w . Indeed, the earlier we relax the constraints (and therefore the higher the initial loss of the eFCN) the further the eFCN escapes from the CNN subspace, as emphasized in Fig. 4 (middle). However, even at early relax times, the eFCNs stay rather close to the CNN subspace, since the ratio never exceeds 8%, whereas it is around 97% for a regular FCN (since the number of off-local weights is much larger than the number of local weights). This underlines the *persistence of the architectural bias under the stochastic gradient dynamics*.

Fig. 4 (right) shows that when we move away from the CNN subspace, performance stays high then plummets down to FCN level. *This hints to a critical distance from the CNN subspace within which eFCNs behave like CNNs, and beyond which they fall back to the standard FCN regime*. We further explore this high performance vicinity of the CNN subspace using interpolations in weight space in Sec. C of the Supplemental Material.

4.4 What role do the extra degrees of freedom play in learning?

How can the eFCN use the extra degrees of freedom to improve performance? From Fig. 5, we see that the off-local part of the eFCN is useless on its own (with the local part masked off). However, when combined with the local part, it may greatly improve performance when the constraints are relaxed early enough. This hints to the fact that the local and off-local parts are performing complementary tasks.

To understand what tasks the two parts they are performing, we show in Fig. 6 a “filter” from the first layer of the eFCN (whose receptive field is of the size of the images since locality is relaxed). Note that each CNN filter gives rise to many eFCN filters : one for each position of the CNN filter on the image, since weight sharing is relaxed. Here we show the one obtained when the CNN filter (local block) is on the top left of the image. We see that off-local blocks stay orders of magnitude smaller than the local blocks, as expected from Sec. 4.3 where we saw that locality was almost conserved. We also see that local blocks hardly change during training, showing that weight sharing of the local blocks is also almost conserved.

More surprisingly, we see that for $t_w > 0$ distinctive shapes of the images are learned by the eFCN off-local blocks, which perform some kind of template-matching. Note that the silhouettes are particularly clear for the intermediate relax time (middle row), at which we know from Sec. 4.1 that the eFCN had the best improvement over the CNN. *Hence, the eFCN is combining template-matching with convolutional feature extraction in a complementary way*.

Note that by itself, template-matching is very inefficient for complicated and varied images such as those of the CIFAR-10 dataset. Hence it cannot be observed in standard FCNs, as shown in Fig. 7 where we reproduce the counterpart of Fig. 6 for the FCN in the left and middle images (they correspond to initial and final training times respectively). To reveal the silhouettes learned, we need to look at the pixelwise difference between the two images, i.e. focus on the change due to training (this is unnecessary for the eFCN whose off-local weights started at zero). In the right image of Fig. 7), we see that a loose texture emerges, however, it is not as sharp as that of the eFCN weights after training. Template-matching is only useful as a cherry-on-the-cake alongside more efficient learning procedures.

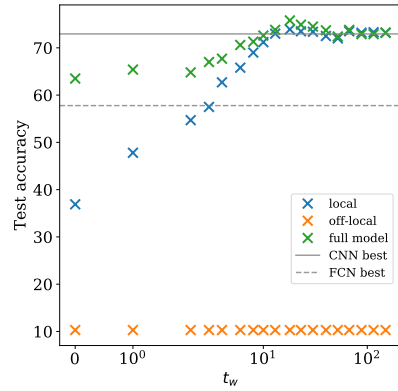


Figure 5: Contributions to the test accuracy of the local blocks (off-local blocks masked out), in orange, and off-local blocks (local blocks masked out), in blue. Combining them together yields a large gain in performance for the eFCN, in green.

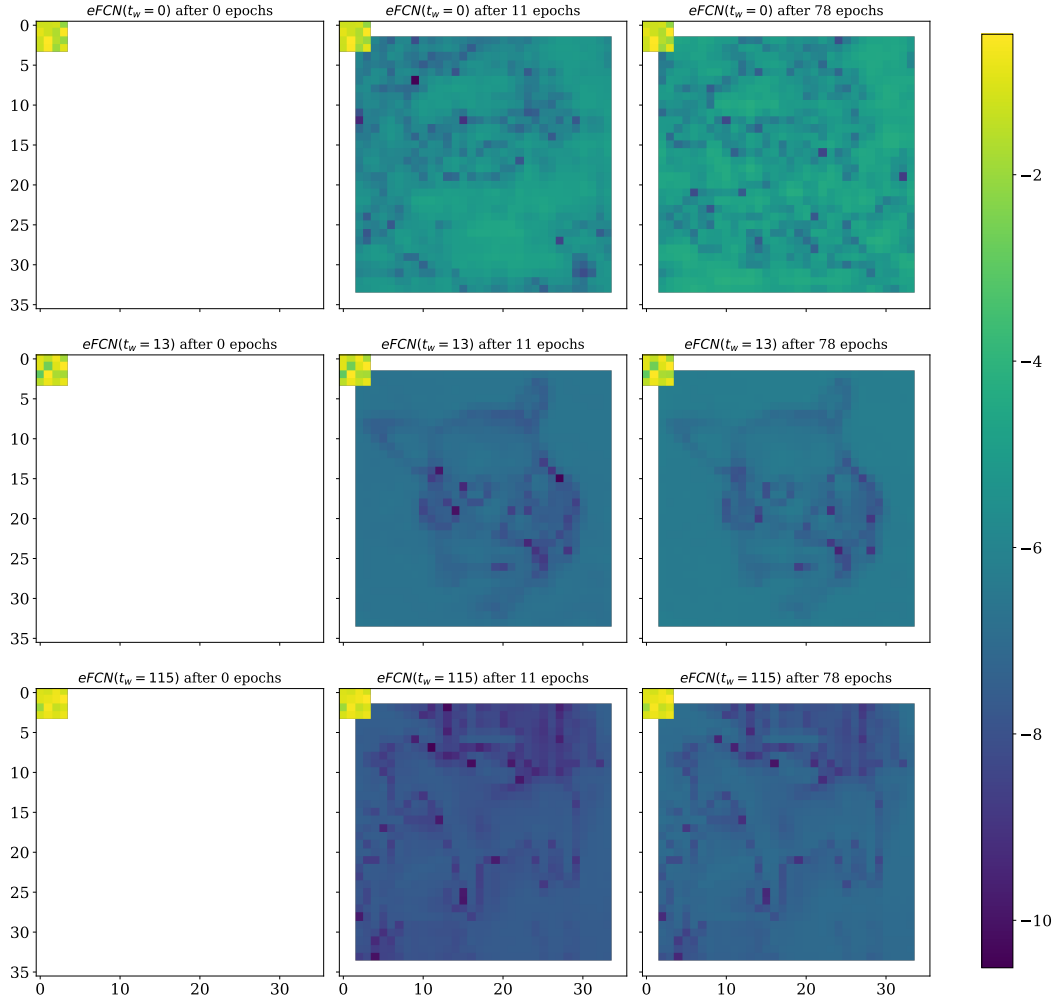


Figure 6: Heatmap of the weights of an eFCN “filter” from the first layer just at relax time (**left** column), after training for 11 epochs (**middle** column), and after training for 78 epochs (**right** column). The eFCNs were initialized at relax times $t_w = 0$ (**top** row), $t_w = 13$ (**middle** row), and $t_w = 115$ (**bottom** row). The colors indicate the natural logarithm of the absolute value of the weights. Note that the convolutional filters, in the top right, vary little and remain orders of magnitude larger than the off-local blocks, whereas the off-local blocks pick up strong signals from images as sharp silhouettes appear.

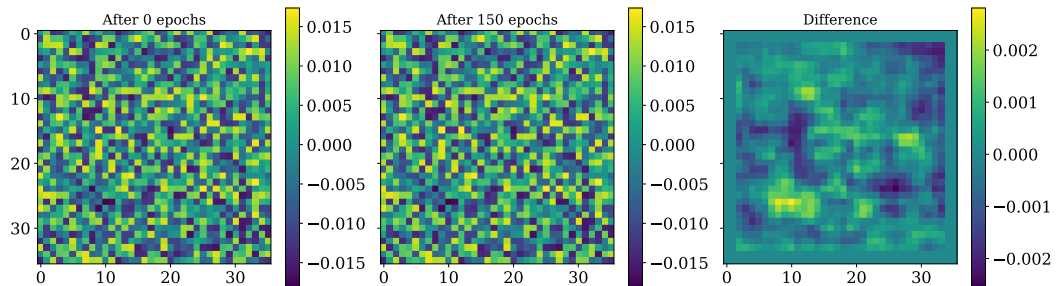


Figure 7: Same heatmap of weights as shown in Fig. 6 but for a standard FCN at a randomly initialized point (**left**) and after training for 150 epochs (**middle**). The pixelwise difference is shown on the **right** panel. A loose texture appears, but it is by no means as sharp as the silhouettes of the eFCNs.

5 Discussion and Conclusion

In this work, we examined the inductive bias of CNNs, and challenged the accepted view that FCNs are unable to generalize as well as CNNs on visual tasks. Specifically, we showed that the CNN prior is mainly useful during the early stages of training, to prevent the unconstrained FCN from falling prey of spurious solutions with poor generalization too early.

Our experimental results show that there exists a vicinity of the CNN subspace with high generalization properties, and one may even enhance the performance of CNNs by exploring it, if one relaxes the CNN constraints at an appropriate time during training. The extra degrees of freedom are used to perform complementary tasks which alone are unhelpful. This offers interesting theoretical perspectives, in relation to other high-dimensional estimation problems, such as in spiked tensor models [2], where a smart initialization, containing prior information on the problem, is used to provide an initial condition that bypasses the regions where the estimation landscape is “rough” and full of spurious minima.

On the practical front, despite the performance gains obtained, our algorithm remains highly impractical due to the large number of degrees of freedom required on our eFCNs. However, more efficient strategies that would involve a less drastic relaxation of the CNN constraints (e.g., relaxing the weight sharing but keeping the locality constraint such as locally-connected networks [11]) could be of potential interest to practitioners.

Acknowledgments

We would like to thank Riza Alp Guler and Ilija Radosavovic for helpful discussions. We acknowledge funding from the Simons Foundation (#454935, Giulio Biroli). JB acknowledges the partial support by the Alfred P. Sloan Foundation, NSF RI-1816753, NSF CAREER CIF 1845360, and Samsung Electronics.

References

- [1] Alessandro Achille, Matteo Rovere, and Stefano Soatto. Critical learning periods in deep neural networks. *arXiv preprint arXiv:1711.08856*, 2017.
- [2] Anima Anandkumar, Yuan Deng, Rong Ge, and Hossein Mobahi. Homotopy analysis for tensor pca. *arXiv preprint arXiv:1610.09322*, 2016.
- [3] Sanjeev Arora, Nadav Cohen, and Elad Hazan. On the optimization of deep networks: Implicit acceleration by overparameterization. *arXiv preprint arXiv:1802.06509*, 2018.
- [4] Jimmy Ba and Rich Caruana. Do deep nets really need to be deep? In *Advances in neural information processing systems*, pages 2654–2662, 2014.
- [5] Carlo Baldassi, Christian Borgs, Jennifer T Chayes, Alessandro Ingrosso, Carlo Lucibello, Luca Saglietti, and Riccardo Zecchina. Unreasonable effectiveness of learning neural networks: From accessible states and robust ensembles to basic algorithmic schemes. *Proceedings of the National Academy of Sciences*, 113(48):E7655–E7662, 2016.
- [6] Carlo Baldassi, Fabrizio Pittorino, and Riccardo Zecchina. Shaping the learning landscape in neural networks around wide flat minima. *arXiv preprint arXiv:1905.07833*, 2019.
- [7] Mikhail Belkin, Daniel Hsu, Siyuan Ma, and Soumik Mandal. Reconciling modern machine learning and the bias-variance trade-off. *arXiv preprint arXiv:1812.11118*, 2018.
- [8] Cristian Buciluă, Rich Caruana, and Alexandru Niculescu-Mizil. Model compression. In *Proceedings of the 12th ACM SIGKDD international conference on Knowledge discovery and data mining*, pages 535–541. ACM, 2006.
- [9] Pratik Chaudhari, Anna Choromanska, Stefano Soatto, Yann LeCun, Carlo Baldassi, Christian Borgs, Jennifer Chayes, Levent Sagun, and Riccardo Zecchina. Entropy-sgd: Biasing gradient descent into wide valleys. *arXiv preprint arXiv:1611.01838*, 2016.
- [10] Tianqi Chen, Ian Goodfellow, and Jonathon Shlens. Net2net: Accelerating learning via knowledge transfer. *arXiv preprint arXiv:1511.05641*, 2015.
- [11] Adam Coates and Andrew Y Ng. Selecting receptive fields in deep networks. In *Advances in neural information processing systems*, pages 2528–2536, 2011.
- [12] Felix Draxler, Kambis Veschgini, Manfred Salmhofer, and Fred A Hamprecht. Essentially no barriers in neural network energy landscape. *arXiv preprint arXiv:1803.00885*, 2018.
- [13] Simon S Du, Jason D Lee, Yuandong Tian, Barnabas Póczos, and Aarti Singh. Gradient descent learns one-hidden-layer cnn: Don’t be afraid of spurious local minima. *arXiv preprint arXiv:1712.00779*, 2017.
- [14] Simon S Du, Yining Wang, Xiyu Zhai, Sivaraman Balakrishnan, Ruslan R Salakhutdinov, and Aarti Singh. How many samples are needed to estimate a convolutional neural network? In *Advances in Neural Information Processing Systems*, pages 373–383, 2018.
- [15] Jonathan Frankle and Michael Carbin. The lottery ticket hypothesis: Finding sparse, trainable neural networks. *arXiv preprint arXiv:1803.03635*, 2018.
- [16] C Daniel Freeman and Joan Bruna. Topology and geometry of deep rectified network optimization landscapes. *arXiv preprint arXiv:1611.01540*, 2016.

- [17] Timur Garipov, Pavel Izmailov, Dmitrii Podoprikhin, Dmitry P Vetrov, and Andrew G Wilson. Loss surfaces, mode connectivity, and fast ensembling of dnns. In *Advances in Neural Information Processing Systems*, pages 8789–8798, 2018.
- [18] Mario Geiger, Arthur Jacot, Stefano Spigler, Franck Gabriel, Levent Sagun, Stéphane d’Ascoli, Giulio Biroli, Clément Hongler, and Matthieu Wyart. Scaling description of generalization with number of parameters in deep learning. *arXiv preprint arXiv:1901.01608*, 2019.
- [19] Mario Geiger, Stefano Spigler, Stéphane d’Ascoli, Levent Sagun, Marco Baity-Jesi, Giulio Biroli, and Matthieu Wyart. The jamming transition as a paradigm to understand the loss landscape of deep neural networks. *arXiv preprint arXiv:1809.09349*, 2018.
- [20] Aditya Golatkar, Alessandro Achille, and Stefano Soatto. Time matters in regularizing deep networks: Weight decay and data augmentation affect early learning dynamics, matter little near convergence. *arXiv preprint arXiv:1905.13277*, 2019.
- [21] Suriya Gunasekar, Jason Lee, Daniel Soudry, and Nathan Srebro. Characterizing implicit bias in terms of optimization geometry. *arXiv preprint arXiv:1802.08246*, 2018.
- [22] Song Han, Huizi Mao, and William J Dally. Deep compression: Compressing deep neural networks with pruning, trained quantization and huffman coding. *arXiv preprint arXiv:1510.00149*, 2015.
- [23] Geoffrey Hinton, Oriol Vinyals, and Jeff Dean. Distilling the knowledge in a neural network. *arXiv preprint arXiv:1503.02531*, 2015.
- [24] Stanisław Jastrzebski, Zachary Kenton, Devansh Arpit, Nicolas Ballas, Asja Fischer, Yoshua Bengio, and Amos Storkey. Three factors influencing minima in sgd. *arXiv preprint arXiv:1711.04623*, 2017.
- [25] Nitish Shirish Keskar, Dheevatsa Mudigere, Jorge Nocedal, Mikhail Smelyanskiy, and Ping Tak Peter Tang. On large-batch training for deep learning: Generalization gap and sharp minima. *arXiv preprint arXiv:1609.04836*, 2016.
- [26] Alex Krizhevsky and Geoffrey Hinton. Learning Multiple Layers of Features from Tiny Images. *Technical Report*, pages 1–60, 2009.
- [27] Alex Krizhevsky, Ilya Sutskever, and Geoffrey E Hinton. Imagenet classification with deep convolutional neural networks. In *Advances in neural information processing systems*, pages 1097–1105, 2012.
- [28] Jaeho Lee and Maxim Raginsky. Learning finite-dimensional coding schemes with nonlinear reconstruction maps. *arXiv preprint arXiv:1812.09658*, 2018.
- [29] Philip M Long and Hanie Sedghi. Size-free generalization bounds for convolutional neural networks. *arXiv preprint arXiv:1905.12600*, 2019.
- [30] Brady Neal, Sarthak Mittal, Aristide Baratin, Vinayak Tantia, Matthew Scicluna, Simon Lacoste-Julien, and Ioannis Mitliagkas. A modern take on the bias-variance tradeoff in neural networks. *arXiv preprint arXiv:1810.08591*, 2018.
- [31] Behnam Neyshabur, Zhiyuan Li, Srinadh Bhojanapalli, Yann LeCun, and Nathan Srebro. Towards understanding the role of over-parametrization in generalization of neural networks. *arXiv preprint arXiv:1805.12076*, 2018.
- [32] Roman Novak, Lechao Xiao, Jaehoon Lee, Yasaman Bahri, Greg Yang, Jiri Hron, Daniel A Abolafia, Jeffrey Pennington, and Jascha Sohl-Dickstein. Bayesian deep convolutional networks with many channels are gaussian processes. *arXiv preprint arXiv:1810.05148*, 2018.
- [33] Steven J Nowlan and Geoffrey E Hinton. Simplifying neural networks by soft weight-sharing. *Neural computation*, 4(4):473–493, 1992.
- [34] Levent Sagun, Utku Evci, V. Uğur Güney, Yann Dauphin, and Léon Bottou. Empirical analysis of the hessian of over-parametrized neural networks. *ICLR 2018 Workshop Contribution*, *arXiv:1706.04454*, 2017.

- [35] Shreyas Saxena and Jakob Verbeek. Convolutional neural fabrics. In *Advances in Neural Information Processing Systems*, pages 4053–4061, 2016.
- [36] Daniel Soudry, Elad Hoffer, Mor Shpigel Nacson, Suriya Gunasekar, and Nathan Srebro. The implicit bias of gradient descent on separable data. *Journal of Machine Learning Research*, 19(70), 2018.
- [37] Luca Venturi, Afonso Bandeira, and Joan Bruna. Neural networks with finite intrinsic dimension have no spurious valleys. *arXiv preprint arXiv:1802.06384*, 2018.
- [38] Lei Wu, Zhanxing Zhu, et al. Towards understanding generalization of deep learning: Perspective of loss landscapes. *arXiv preprint arXiv:1706.10239*, 2017.
- [39] Chiyuan Zhang, Samy Bengio, Moritz Hardt, Benjamin Recht, and Oriol Vinyals. Understanding deep learning requires rethinking generalization. *arXiv preprint arXiv:1611.03530*, 2016.

A Visualizing the embedding

In Fig. 8, we provide an illustration of the mapping from CNN to eFCN. Denoting as k, s, p the filter size, stride and padding of the convolution, we have the following:

$$\begin{aligned}
 d_{in} &= 4 \\
 (k, s, p) &= (3, 1, 0) \\
 d_{out} &= \frac{d_{in} + 2p - k}{s} + 1 = 2
 \end{aligned}$$

The eFCN layer is of size $(c_{in} \times d_{in} \times d_{in}, c_{out} \times d_{out} \times d_{out}) = (4, 16)$ since $c_{in} = c_{out} = 1$ here. In Fig. 9, we show the typical structure of the eFCN weight matrices observed in practice.

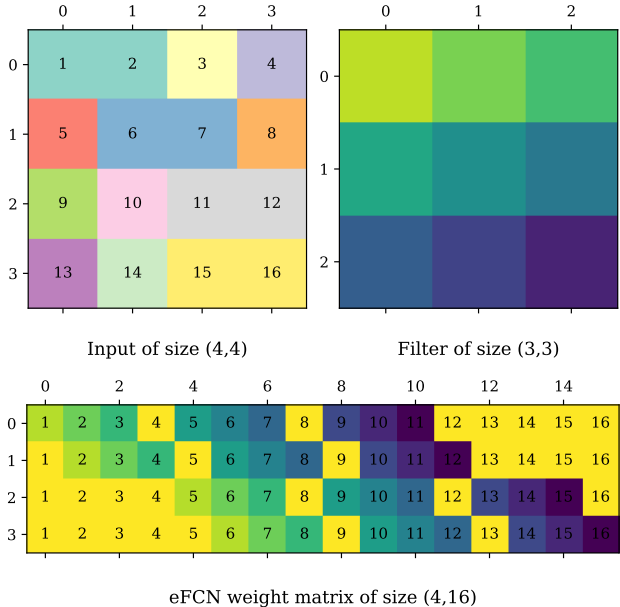


Figure 8: eFCN wight matrix (**bottom**) obtained when acting on an input of size of size (4,4) (**top left**) with a filter of size (3,3) (**top right**). The colors of the eFCN weight matrix show where they stem from in the filter (the off-local blocks, in yellow, are set to zero at initialization).

B Results with AlexNet on CIFAR-100

In this section, we show that the ideas we presented in the main text hold for various classes of data, architecture and optimizer. Namely, we show that our results hold when switching from SGD to Adam on CIFAR10, and for AlexNet [27] on the CIFAR-100 dataset. Each subsection contains figures which are counterparts of the ones of the main text : performance and training dynamics of the eFCNs in Fig. 10, deviation from CNN subspace in Fig. 11, role of off-local blocks in learning in Fig. 12.

C Interpolating between CNNs and eFCNs

Another way to understand the dynamics of the eFCNs is to examine the paths that connect them to the CNN they stemmed from in the FCN weight space. Interpolating in the weight space has received some attention in recent literature, in papers such as [12, 17], where it has been shown that contrary to previous beliefs the bottom of the landscapes of deep neural networks resembles a flat, connected level set since one can always find a path of low energy connecting minima.

Here we use two interpolation methods in weight space. The first method, labeled "linear", consists in sampling n equally spaced points along the linear path connecting the weights. Of course, the interpolated points generally have higher training loss than the endpoints.

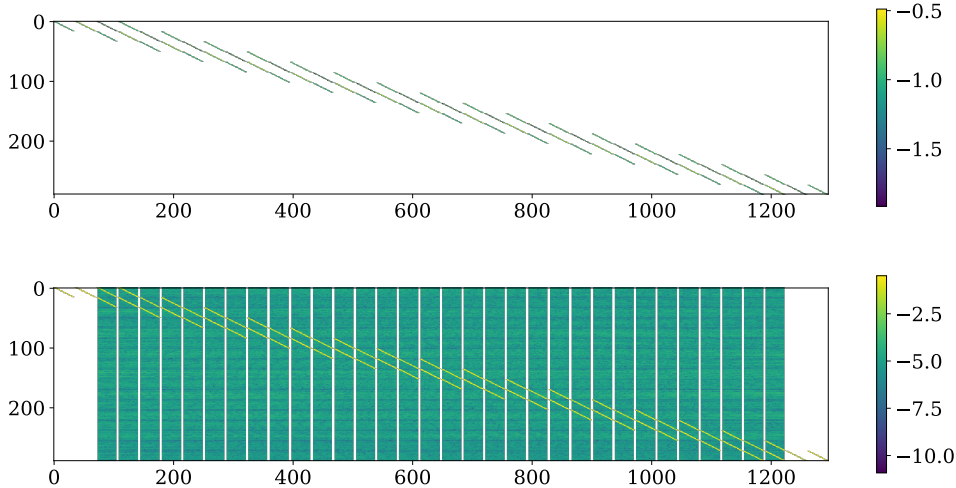


Figure 9: **Top:** Heatmap of a block of weights corresponding to the first input channel and the first output channel of the first layer of the eFCN just after its initialization from the converged VanillaCNN. The colorscale indicates the natural logarithm of the absolute value of the weights. The highly sparse and self-repeating structure of the weight matrix is due to the locality and weight sharing constraints. **Bottom:** Same after training the eFCN for 100 epochs. The off-local blocks appear in blue : their weights are several orders of magnitude smaller in absolute value than those of the local blocks, in yellow. Note that due to the padding many weights stay at zero even after relaxing the constraints. When unflattened, the first row of this heatmap gives rise to the images shown in Fig. 12.

The second method, labeled "string", consists in starting from the linear interpolation path, and letting the interpolated points fall down the landscape following gradient descent, while ensuring that they stay close enough together by adding an elastic term in the loss :

$$\mathcal{L}_{elastic} = \frac{1}{2}k \sum_{i=1}^{n-1} (\mathbf{x}_{i+1} - \mathbf{x}_i)^2 \quad (2)$$

By adjusting the stiffness constant k we can control how straight the string is: at high k we recover the linear interpolation, whereas at low k the points decouple and reach the bottom of the landscape, but are far apart and don't give us an actual path. Note that this method is a simpler form of the one used in [12], where we don't use the "nudging" trick.

For comparison, we also show the performance obtained when interpolating directly in output space (as done in ensembling methods).

Results are shown in figure 13, with the x -axis representing the interpolation parameter $\alpha \in [0, 1]$. We see that for both the linear and string interpolations, the training loss profile displays a barrier, except at late t_w where the eFCN has not escaped far from the CNN subspace. Although the string method fails to find a path without a barrier, this is not sufficient to conclude that no paths exist.

However, the behavior of test accuracy is much more surprising. In all cases, despite the increase in training loss, the interpolated paths reach higher test accuracies than the endpoints, even at early t_w when the eFCN and the CNN are quite far from each other. This confirms that there is a basin of high generalization around the CNN subspace, and that optimum performance can actually be found somewhere in between the solution found by the CNN and the solution found by the eFCN. This offers yet another procedure to improve the performance in practice. However, in all cases we note that the gain in accuracy is lower than the gain obtained by interpolating in output space.

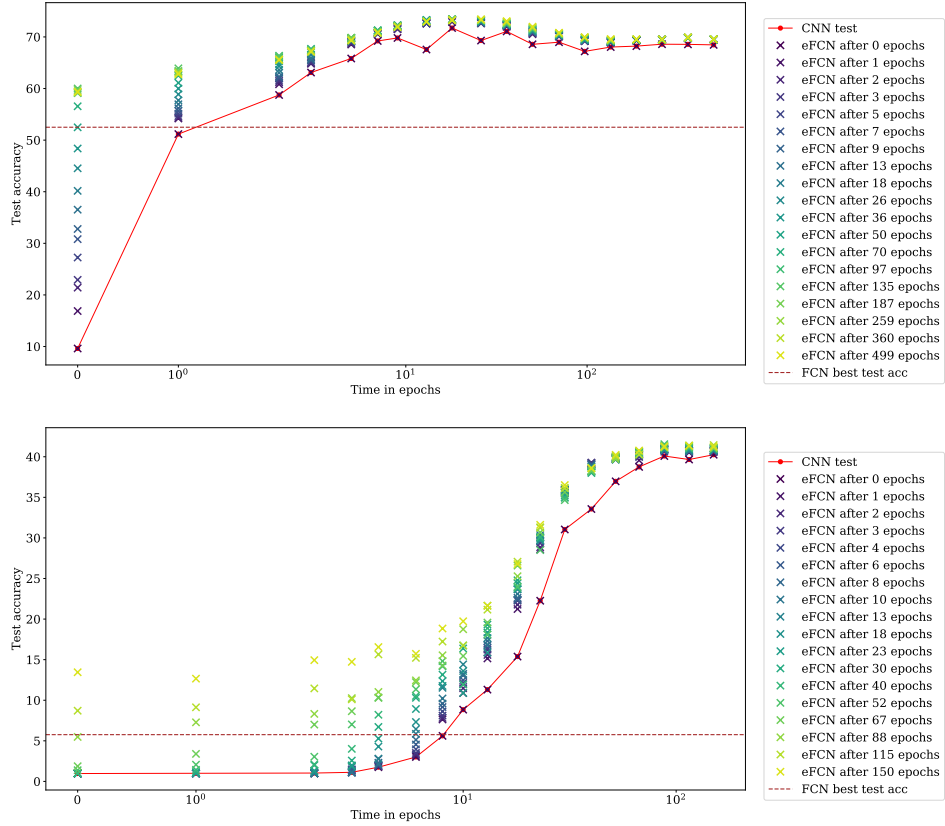


Figure 10: This figure sums up in a compact way the generalization dynamics of the eFCNs. The red curve represents the test accuracy of the model versus its training time in epochs. Above each point t_w of the training, we depict as crosses the test accuracy history of the eFCN stemmed at relax time t_w , with colors indicating the training time of the eFCN after embedding. For comparison, the best test accuracy reached by a standard FCN of same size is depicted as a brown horizontal dashed line. **Left:** VanillaCNN on CIFAR-10, with Adam optimizer. **Right:** Alexnet on CIFAR-100, with SGD optimizer. We note that results are qualitatively similar: the eFCNs always improve after initialization, outperform the standard FCN, and we again observe that for some relax times the eFCNs even exceeds the best test accuracy reached by the CNN.

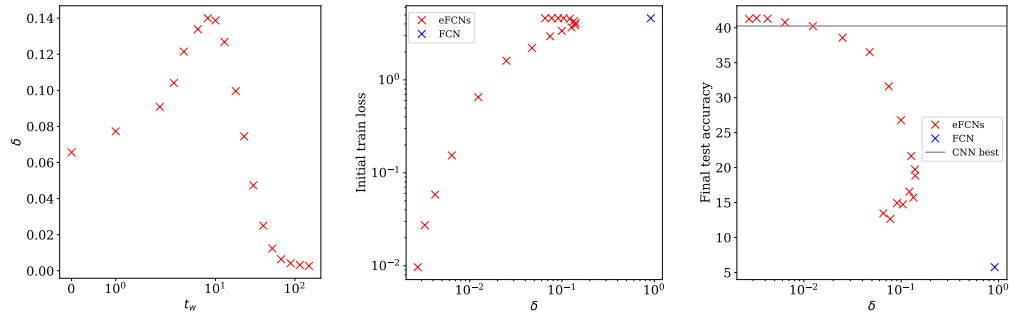


Figure 11: **Left panel:** relax time t_w of the eFCN vs. δ , the measure of deviation from the CNN subspace through the locality constraint, at the final point of eFCN training. **Middle panel:** δ vs. the initial loss value. **Right panel:** δ vs. final test accuracy of eFCN models. For reference, the blue point in the **middle** and **right** panels indicate the deviation measure for a standard FCN, where $\delta \sim 97\%$.

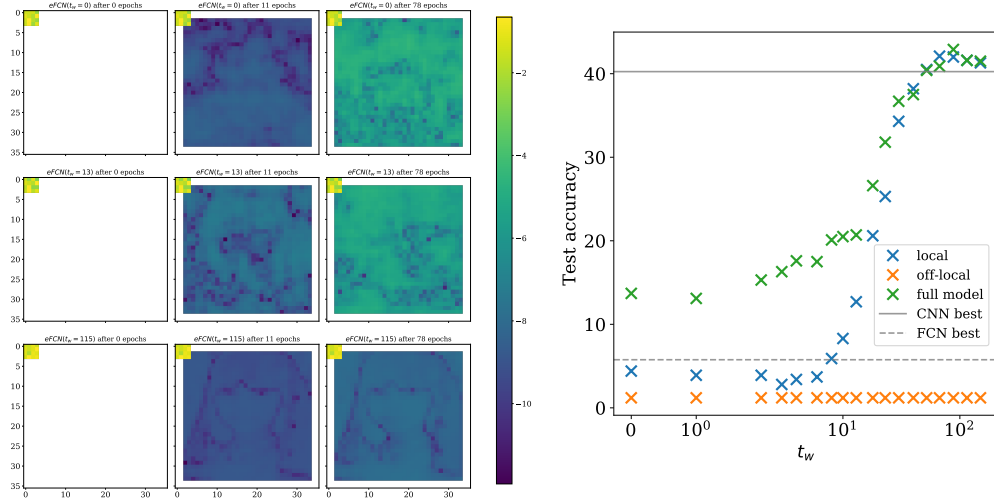


Figure 12: **Left:** Visualization of an eFCN “filter” from the the first layer just after embedding (left column), after training after 11 epochs (middle column), and training after 78 epochs (right column); where the eFCN is initialized at relax times $t_w = 0$ (top row), $t_w = 13$ (middle row), and $t_w = 115$ (bottom row). The colors indicate the natural logarithm of the absolute value of the weights. **Right:** Contributions to the test accuracy of the local blocks (off-local blocks masked out) and off-local blocks (local blocks masked out).

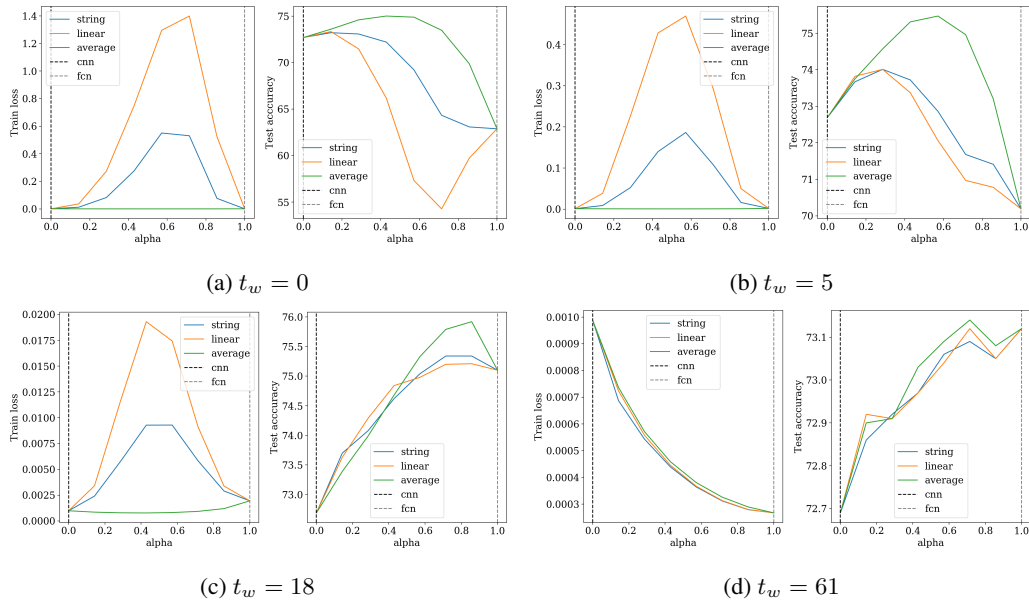


Figure 13: Interpolation between the solution reached by the CNN after 100 epochs (interpolation parameter $\alpha = 0$) and the solution found by the eFCN after 100 epochs (interpolation parameter $\alpha = 1$), for four different relax times t_w indicated below the subfigures. In each subfigure, the **left** panel shows train loss, and the **right** panel shows test accuracy. The orange line corresponds to linear interpolation, the blue line corresponds to string method interpolation, and the green line corresponds to interpolation in output space.